PNAS RESEARCH ARTICLE | CELL BIOLOGY OPEN ACCESS

An aggregated mitochondrial distribution in preimplantation embryos disrupts nuclear morphology, function, and developmental potential

In-Won Lee[a], Abbas Pirpour Tazehkand[a], Zi-Yi Sha[a], Deepak Adhikari[a,1], and John Carroll[a,1]

Affiliations are included on p. 10.

Edited by Kathy Niakan, University Cambridge Center for Trophoblast Research, Cambridge, United Kingdom; received October 13, 2023; accepted May 23, 2024 by Editorial Board Member Brigid L. Hogan

A dispersed cytoplasmic distribution of mitochondria is a hallmark of normal cellular organization. Here, we have utilized the expression of exogenous *Trak2* in mouse oocytes and embryos to disrupt the dispersed distribution of mitochondria by driving them into a large cytoplasmic aggregate. Our findings reveal that aggregated mitochondria have minimal impact on asymmetric meiotic cell divisions of the oocyte. In contrast, aggregated mitochondria during the first mitotic division result in daughter cells with unequal sizes and increased micronuclei. Further, in two-cell embryos, microtubule-mediated centering properties of the mitochondrial aggregate prevent nuclear centration, distort nuclear shape, and inhibit DNA synthesis and the onset of embryonic transcription. These findings demonstrate the motor protein-mediated distribution of mitochondria throughout the cytoplasm is highly regulated and is an essential feature of cytoplasmic organization to ensure optimal cell function.

mitochondrial aggregation | Nuclear morphology | TRAK2 | Meiosis | Mitosis

Significance

Mitochondria are one of the most abundant organelles in the cell and are typically dispersed throughout the cytoplasm. It is not known whether this distribution is essential for normal cell function or whether it is simply a reflection of the balance of motor protein activity. We find that disrupting this mitochondrial distribution by promoting mitochondrial aggregation in mouse oocytes is without effect, but in embryos leads to dramatic effects on nuclear localization, shape, and function. The resultant inhibition of DNA replication, increase in DNA damage, and suppression of transcription result in compromised preimplantation development. Our findings reveal a role of maintaining a dispersed mitochondrial distribution in regulating nuclear dynamics and function in early embryo development.

Mitochondrial biogenesis and quality control are achieved by fission and fusion, the balance of which at any moment in time determines overall mitochondrial morphology (1, 2). This ranges from individual mitochondria 1 to 5 μm in length, thorough to an interconnected cytoplasmic network. Typically, mitochondria are dispersed throughout the cytoplasm, which is achieved via active trafficking on the cytoskeletal network by dynein, kinesin, and myosin-based motor proteins (3, 4). This trafficking is highly regulated and associated with changes in the cell cycle (5, 6), energy demand (7), and cell movement (8, 9). Although this highly dispersed mitochondrial distribution is typical of most cell types, large or highly specialized cells, such as neurons, sperm, and oocytes, often show aggregation of mitochondria in specific cytoplasmic compartments. This targeted distribution may be important for meeting local energy demands at the synapse (10) or meiotic spindle (11–15) or for ensuring optimal mitochondrial distribution into daughter cells at cell division (1, 14, 16, 17).

Maintaining this dynamic regulated distribution of mitochondria requires a complex interaction between motor proteins, the actin and microtubule (MT)-based cytoskeleton, and adaptor proteins that link mitochondria to the motors (3, 18). MT-mediated trafficking via Dynein and Kinesin-1 is largely responsible for trafficking mitochondria throughout the cytoplasm (19), while actin-coupled myosin-based motors are responsible for short-range movement and mitochondrial positioning (20, 21). The ability of dynein and kinesin to traffic mitochondria is mediated via the adapter protein TRAK1/2, which couples the motor protein to mitochondria via the outer mitochondrial membrane protein, MIRO1/2 (22–30). TRAK (Milton in Drosophila) loss of function studies reveal disrupted accumulation of mitochondria in synapses leading to aberrant synaptic transmission (10, 25, 31), while in Drosophila oogenesis loss of TRAK leads to the absence of the Balibani body and the failure to accumulate mitochondria in the oocyte (32). These studies and others indicate that distinct cellular events such as synaptic transmission and germ cell formation require a specific distribution of mitochondria, yet it is not clear whether the typical dispersed mitochondrial distribution seen in most cell types is essential for cellular function, or if the distribution pattern is simply a manifestation of the intrinsic properties of motor proteins and adaptors.

Mammalian oocytes are the largest cells in the body and typically contain 200,000—400,000 mitochondria (33–35). They are an ideal model for investigating the role of mitochondrial trafficking as oocyte mitochondria undergo major changes in distribution and function during the highly asymmetric divisions of oocyte meiosis (14, 36). Following

Author contributions: I.-W.L., D.A., and J.C. designed research; I.-W.L. performed research; I.-W.L. contributed new reagents/analytic tools; I.-W.L., A.P.T., and Z.-Y.S. analyzed data; and I.-W.L., D.A., and J.C. wrote the paper.

The authors declare no competing interest.

This article is a PNAS Direct Submission. K.N. is a guest editor invited by the Editorial Board.

[1]To whom correspondence may be addressed. Email: deepak.adhikari@monash.edu or j.carroll@monash.edu.

This article contains supporting information online at https://www.pnas.org/lookup/suppl/doi:10.1073/pnas.2317316121/-/DCSupplemental.

Published June 25, 2024.

fertilization, mitochondria distribute homogeneously throughout the cytoplasm before being distributed evenly into the two daughter cells of the first mitotic division. Mitochondrial activity in oocytes is also spatially regulated (16) and disrupting mitochondrial function causes meiotic arrest and fertilization failure (37, 38). Interventions that lead to altered mitochondrial distribution are associated with compromised oocyte maturation or embryo development (39–42), while specific disruption of mitochondrial trafficking via oocyte-specific deletion of MIRO1, leads to modest changes in mitochondrial organization and rates of meiotic progression (42). Furthermore, in human preimplantation embryos, aggregated, or uneven mitochondrial distribution is associated with compromised IVF outcomes (43).

Here, we have used a gain-of-function approach to directly examine the role of mitochondrial distribution in mouse oocytes and early embryos. Expression of the adaptor protein, TRAK2, in mouse oocytes and early embryos, in line with its known role in enhancing Dynein-mediated trafficking (27), leads to a dramatic aggregation of mitochondria into a large cytoplasmic ball. This provides a model system to investigate the fundamental question of how mitochondrial distribution impacts on the specialized cell divisions of oocytes and early embryos. We find that the extreme asymmetric meiotic cell divisions in oocytes are relatively unaffected by mitochondrial aggregation. However, early mitotic divisions show disrupted symmetry of cell division, compromised nuclear position, shape and function, and inhibition of preimplantation development. These findings show that the typically dispersed distribution of mitochondria is important to ensure nuclear and cellular function compatible with preimplantation development.

Results

***Trak2* Gain of Function Leads to Bidirectional Mitochondrial Redistribution in Germinal Vesicle (GV)-Stage Immature Oocytes.** Analysis of *Trak2* expression in oocytes using published transcriptomic datasets reveals low levels of expression in oocytes and preimplantation datasets (42). This was also evident in previously published proteomic datasets in which TRAK2 was not present among 3,768 identified proteins (44). We therefore turned to using exogenous expression of *Trak2-EGFP* and *myc-Trak2* in an effort to manipulate mitochondrial organization in oocytes and embryos. First, we examined the distribution of TRAK2 in mouse oocytes by expressing *Trak2-EGFP*. TRAK2-EGFP was localized at mitochondria, as indicated by its colocalization with Mitotracker Red (*SI Appendix*, Fig. S1). Interestingly, we also noted in metaphase I (MI)-stage oocytes that TRAK2-EGFP was present between spindle fibers within the meiotic spindle and in two distinct clusters at the spindle pole. Mitochondria were observed to be significantly more aggregated into clusters in *Trak2-EGFP*-expressing oocytes, revealing that exogenous TRAK2 provides a gain-of-function approach for manipulating mitochondrial distribution in mouse oocytes.

First, we injected *myc-Trak2* mRNA into GV-stage oocytes and examined mitochondrial distribution after 3 h. We identified two distinct patterns of mitochondrial distribution (Fig. 1 *A* and *B* and Movie S1). First, a massive mitochondrial aggregation around the GV was observed in approximately 60% of *Trak2*-expressing oocytes (Fig. 1 *A*–*C*, Type1). The second phenotype involved an increase in the clusters of mitochondrial aggregates at the oocyte cortex (Fig. 1 *A*–*C*, Type2). In both cases, the cytoplasm effectively became cleared of mitochondria in favor of the perinuclear or cortical aggregates. Analysis of mitochondrial clusters showed *Trak2*-expressing oocytes had a threefold to fourfold decrease in the number of mitochondrial clusters (Fig. 1*D*) and an approximately sixfold increase in the mean cluster size (Fig. 1*E*).

We investigated the basis for these two patterns of distribution. To control for possible differences in the amount of *Trak2* expressed in individual oocytes, we injected Trak2 mRNA at pipette concentrations of 300 ng/μL (standard), 150 ng/μL, and 75 ng/μL. This showed that while >95% of oocytes injected with 300 ng/μL showed aggregated mitochondria (Type1 or Type2), lower pipette concentrations induced aggregation in only 60% and 20% of oocytes, respectively (*SI Appendix*, Fig. S2). Interestingly, the proportion of oocytes showing a Type1 or Type2 pattern of aggregation was not impacted by mRNA concentration. We conclude that, while mitochondrial aggregation per se is *Trak2*-concentration dependent, the pattern of aggregation is not.

Next we tested whether the aggregation pattern was related to the diameter of the oocyte. Oocytes were typically collected from prepubertal 21 to 23 d-old mice to maximize the number of eggs recovered (45). Oocytes from these young mice are slightly smaller (typically 67.5 μm in diameter) than oocytes from mice at 6 wk of age (71.0 μm in diameter) (Fig. 1*G*). Comparing the pattern of mitochondrial aggregation (Fig. 1*F*) revealed oocytes from 3 wk-old mice predominantly displayed perinuclear mitochondrial distribution (Type1), whereas oocytes from 6-wk-old mice showed cortically aggregated mitochondria (Type2) (Fig. 1*H*). Further analysis of the relationship revealed as oocyte diameter increases the proportion of mitochondria outside the perinuclear region also increases (Fig. 1*I*). Thus, although it remains possible the onset of puberty may alter oocyte physiology, this experiment indicates a strong relationship between oocyte size and the pattern of Trak2-induced mitochondrial distribution.

Massive Mitochondrial Clustering Does Not Affect Mitochondrial Activity. We next measured mitochondrial membrane potential (MMP) to test whether TRAK2-mediated aggregation had any effect on mitochondrial function. Due to differences in mitochondrial distribution, MMP was measured using the ratio of TMRM (MMP-sensitive) and mito-Dendra2 (MMP-insensitive) (16) in *Trak2* expressing and control (vehicle-injected) oocytes. This ratiometric analysis shows that MMP is not affected, despite the dramatic difference in mitochondrial aggregation caused by TRAK2 (Fig. 2 *A* and *B*).

Mitochondrial Aggregation Delays Meiosis Resumption but Not Spindle Organization. During maturation, fully grown oocytes undergo a series of cell cycle transitions, including germinal vesicle breakdown (GVBD), meiotic spindle formation, chromosome segregation, first polar body extrusion and finally, arrest in metaphase of meiosis II (MII) (Fig. 3*A*). This meiotic progression is associated with dramatic changes in mitochondrial distribution (14, 36, 46), which led us to ask whether disrupting mitochondrial distribution using TRAK2 impacts oocyte maturation. *Trak2*-injected oocytes were maintained in meiotic arrest for 3 h to allow for expression, before release and assessment of GVBD two hours after meiotic resumption. At this 2 h time point, a smaller proportion of *Trak2*-injected oocytes had progressed to GVBD than controls (85% vs. 60%, respectively; Fig. 3*B*), but there was no effect on the ability of these oocytes to extrude the first polar body and complete oocyte maturation (Fig. 3*C*). We further tested the effects of *Trak2* expression by extending the period of meiotic arrest from 3 h to 24 h prior to release. Similar to the shorter time frame, allowing 24 h for *Trak2* expression caused a modest inhibition of GVBD and no effect on polar body extrusion compared to vehicle controls (*SI Appendix*, Fig. S3). Thus, while

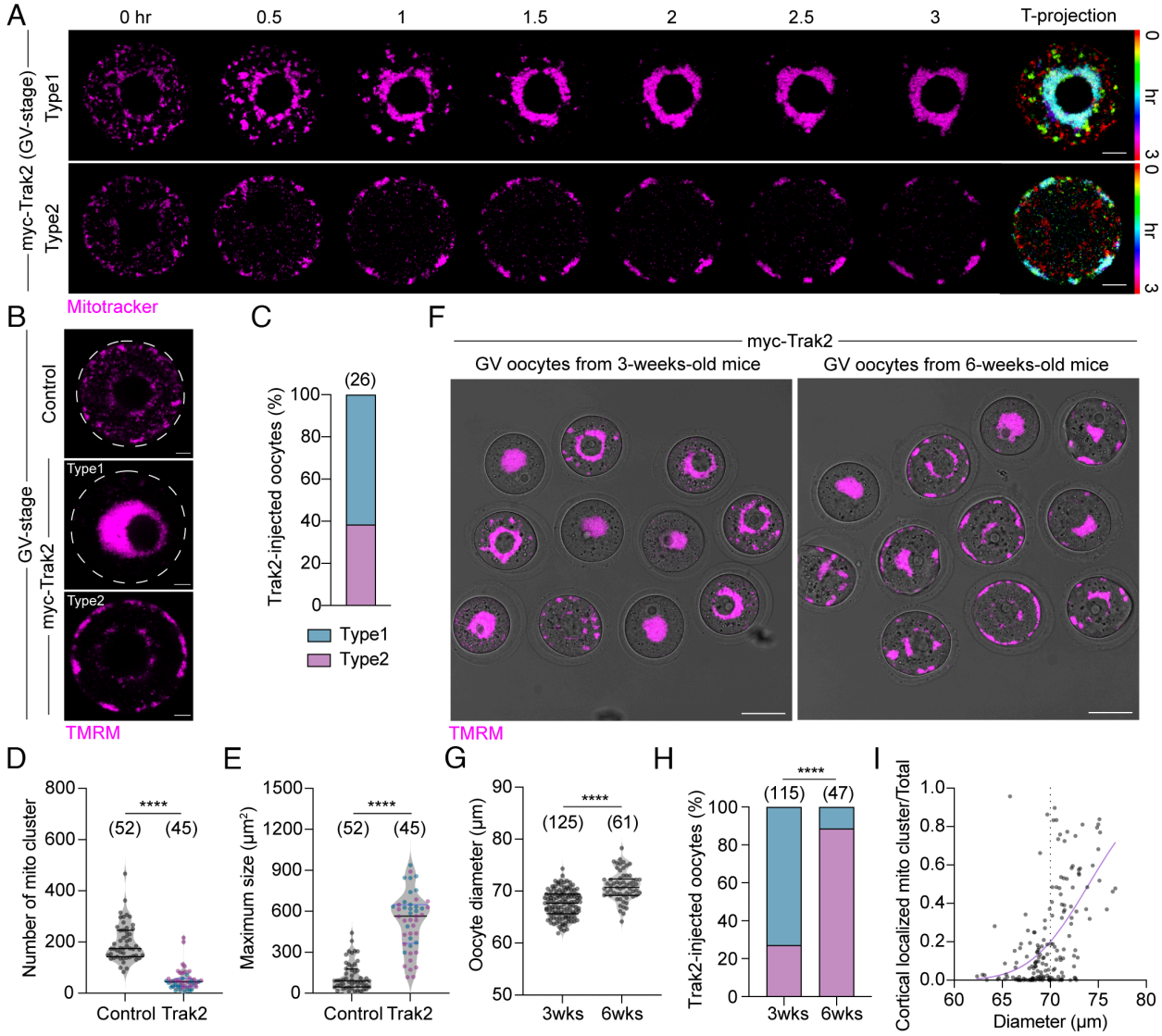

Fig. 1. Exogenous *Trak2* expression promotes bidirectional mitochondrial trafficking in GV oocytes. (*A*) Time-lapse images of two distinct types of mitochondrial redistribution after *myc-Trak2* injection at t = 0. Time projection images are shown with spectrum pseudocolors (four different time points at 0, 1, 2, and 3 h). Type1: Mitochondria aggregation around the GV, Type2: Mitochondria aggregation at the oocyte cortex. (*B*) Representative images of mitochondrial redistribution induced by *Trak2* overexpression. (*C*) The proportion of *Trak2*-expressing oocytes exhibiting Type1 and Type2. (*D* and *E*) Quantification of the number and size of mitochondrial clusters. Unpaired *t* test. (*F*) Representative images of mitochondrial redistribution in *Trak2*-expressing GV oocytes obtained from 3- and 6-wk-old mice. (*G*) Measurement of oocyte diameter obtained from 3- and 6-wk-old mice. Unpaired *t* test. (*H*) The proportion of *Trak2*-expressing oocytes from 3- and 6-wk-old mice showing Type1 and Type2. Chi-square. (*I*) Correlation between oocyte diameter and the area of mitochondria located in the cortex, excluding the perinuclear region. n = 171. Kolmogorov–Smirnov test. Oocytes were collected from 3-wk-old mice for (*A*–*I*) or 6-wk-old mice for (*F*–*I*). Scale bar is 15 μm (*A*), 10 μm (*B*) or 50 μm (*F*). n.s., not significant. ****$P < 0.0001$.

entry into GVBD is delayed/arrested in a proportion of oocytes, in those that undergo GVBD in a timely manner subsequent progress to MII is not affected by the presence of TRAK2 or the induced changes to mitochondrial distribution.

We next examined how mitochondrial distribution is affected by TRAK2 at key stages of oocyte maturation and assessed the effect on spindle formation in MI and MII. In agreement with previous findings (14, 36, 46), mitochondria in control oocytes gradually encircled the developing MI spindle with varying numbers of mitochondrial clusters present in the cytoplasm (Fig. 3 *D* and *E*). At MII, mitochondria typically redistribute through the cytoplasm, but with an increased presence associated with the spindle hemisphere and overlying cortex (Fig. 3 *G* and *H*). In comparison, *Trak2* expression exacerbated the trafficking of mitochondria to the spindle region in MI, essentially clearing the rest of the cytoplasm of mitochondria (Fig. 3 *D* and *E*), while at MII, mitochondria were largely distributed in the central cytoplasm, with no evidence of concentration around the spindle hemisphere and cortex (Fig. 3 *G* and *H*). Despite these differences in mitochondrial distribution at MI and MII, spindle formation appeared unaffected at both stages (Fig. 3 *F* and *I*). Furthermore, no evidence of aneuploidy was found in *Trak2*-injected oocytes (Fig. 3 *G* and *J*), suggesting that increased mitochondrial aggregation around the developing MI spindle and altered distribution at MII has no effect on spindle function in the MI to MII transition.

***Trak2* Overexpression in Zygotes Leads to Unidirectional Mitochondrial Aggregation.** During the asymmetric meiotic division of oocytes, mitochondria are preferentially retained in the oocyte and largely excluded from the first polar body (14). In contrast, the mitotic cell divisions of early embryos aim to segregate mitochondria and other organelles equally to the daughter blastomeres. As such, we hypothesized that the dispersed mitochondrial distribution typical of early embryos may be

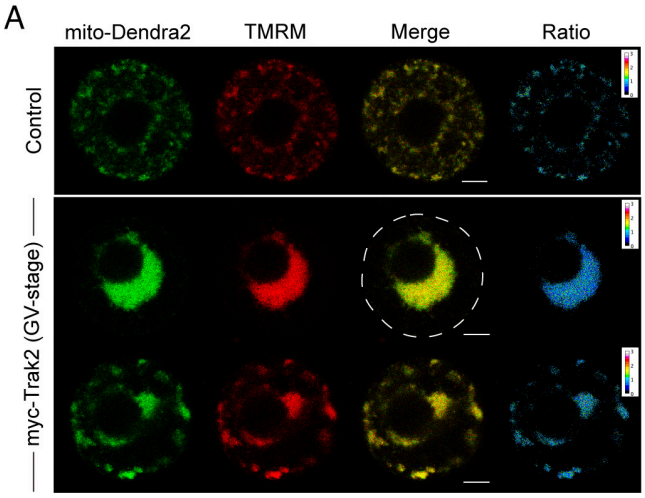

Fig. 2. *Trak2* overexpression does not alter mitochondrial MMP. (*A*) Representative examples of TMRM and mito-Dendra2 in control and *Trak2*-expressing oocytes. Psuedocolor ratiometric images of TMRM and mito-Dendra2 are shown. (*B*) Quantification of the fluorescence intensity ratio of TMRM to mito-Dendra2. The data were normalized by dividing the values of each group by the mean of control oocytes. Unpaired *t* test. Oocytes were collected from 3-wk-old mice. The scale bar is 15 μm (*A*). n.s.; not significant.

essential to facilitate equal mitochondrial inheritance during cell division.

We overexpressed *myc-Trak2* in zygotes collected approximately 12 h postfertilization to examine its impact on mitochondrial distribution. Mitochondria initially began to aggregate into small clusters (*SI Appendix*, Fig. S4), probably around MT asters as we have previously shown in oocytes (14). These cytoplasmic clusters are clearly seen 100 min after *Trak2*-expression and they then

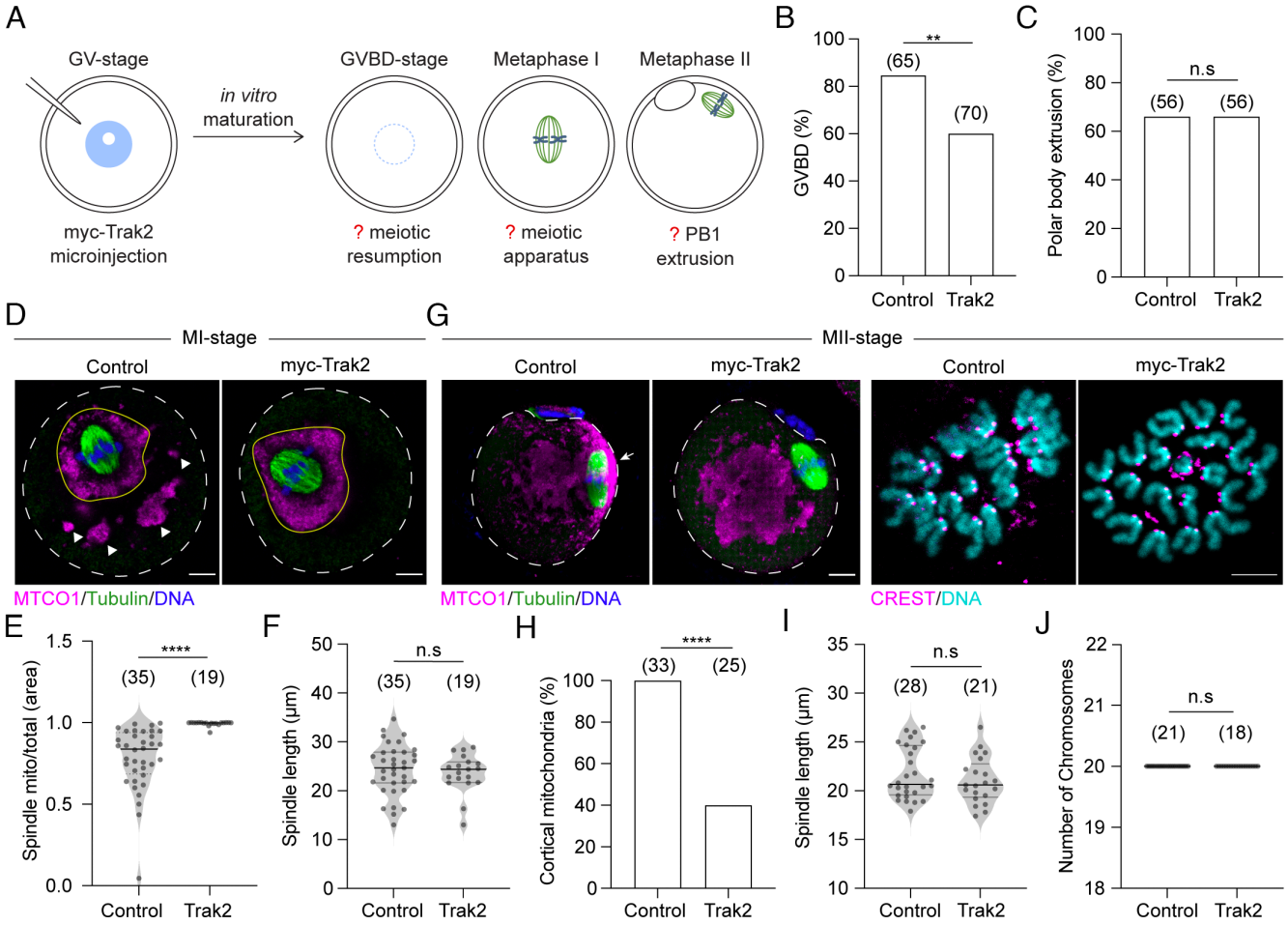

Fig. 3. Mitochondrial aggregation by *Trak2* delays meiotic resumption but not progression to MII. (*A*) A schematic diagram illustrating the analysis performed. (*B*) The percentage of oocytes undergoing NEBD. Chi-square. (*C*) The percentage of MI oocytes extruding the first polar body. Chi-square. (*D*) Representative images of mitochondrial distribution and MI spindles in control and *Trak2*-expressing oocytes. Dashed lines: Oocyte membrane. Yellow lines: Spindle-associated mitochondrial clusters. White arrowheads: Cytoplasmic mitochondrial cluster. (*E*) Ratiometric analysis comparing spindle-associated mitochondrial clusters to total mitochondrial clusters. Unpaired *t* test. (*F*) Measurement of MI spindle length. Unpaired *t* test. (*G*) Representative images of mitochondrial distribution and chromosomes in control and *Trak2*-expressing MII oocytes. Dashed line: Oocyte membrane. White arrow: Cortically localized mitochondria. (*H*) The percentage of oocytes showing cortically localized mitochondria. Chi-square. (*I*) Measurement of MII spindle length. Unpaired *t* test. (*J*) The number of chromosomes in control and *Trak2*-expressing MII oocytes. Unpaired *t* test. Oocytes were collected from 3-wk-old mice for the experiments. The scale bar is 10 μm (*D* and *G*), or 5 μm (*G*, chromosome spreads). n.s., not significant. $^{**}P < 0.01$ and $^{****}P < 0.0001$.

progressively moved toward the central position of the zygote. Interestingly, *Trak2*-injected zygotes showed no evidence of the Type2 cortical distribution observed in GV oocytes (Fig. 1). Instead all zygotes display unidirectional mitochondrial movement, where they aggregate into a large ball-like structure, displacing the pronuclei (PN) at the center of the zygote (Fig. 4*A*, *Right*). To quantify *Trak2*-mediated mitochondrial aggregation in zygotes, we measured the intensity of mito-Dendra2 signals using a Radial Profile Angle (Fig. 4*B*). The length of the radius measuring the integrated intensities across the full 360° was set to 30 µm to account for small size variations observed across the zygote population. In controls, the analysis revealed that mitochondria were homogeneously dispersed throughout the cytoplasm (Fig. 4*C*, blue), while in *Trak2*-expressing zygotes, the intensity of mito-Dendra2 fluorescence was highest at the center and fell dramatically as the radius length increased (Fig. 4*C*, purple). This dramatic aggregation resulted in a small but significant decrease in MMP, although this difference was not apparent 20 h later in two-cell embryos (Fig. 4 *D*–*F*). These data indicate that the egg-to-embryo transition results in a change in the properties of underlying motor protein activity resulting in a dramatic change in the spatial organization of mitochondria.

Mitochondrial Aggregation Disrupts Preimplantation Development. We investigated the impact of *Trak2*-mediated mitochondrial aggregation on preimplantation development and on mitochondrial inheritance in the first mitotic cell division. First, we examined the developmental potential of *Trak2*-injected zygotes to reach the blastocyst stage in vitro. Control zygotes progressed to blastocysts at a rate of 68% compared to only 7% of *Trak2*-injected zygotes (Fig. 5 *A* and *B*).

The vast majority of *Trak2*-injected zygotes formed normal spindles (Fig. 5 *C* and *D*) and progressed to the two-cell stage, suggesting the cytoplasmic mass of mitochondria per se was not incompatible with an apparently normal first mitotic division. We performed time-lapse imaging during the one- to two-cell transition to investigate mitochondrial segregation into daughter cells. First, in control zygotes (Fig. 5*E*, *Upper*, Movie S2), the two PN become centered in the cytoplasm before nuclear envelope breakdown (NEBD) and chromosome alignment on the first mitotic spindle. A proportion of mitochondria concentrate around the mitotic apparatus before being segregated with chromosomes into two daughter blastomeres of the two-cell embryo. In *Trak2*-injected zygotes, the presence of the large ball of mitochondria created a number of challenges in the first mitotic division (Fig. 5*E*, *Bottom*, Movie S2). The mitochondrial mass prevented the centering and apposition of PN, resulting in maternal and paternal chromosomes condensing into separate clusters (*Inset* NEBD). Remarkably, these two sets of chromosomes then migrated to the center of the mitochondrial mass (*Inset* Metaphase). During cell division, the mitochondrial mass extends longitudinally with the segregating chromosomes such that at cytokinesis the mitochondria were divided into the two daughter blastomeres (*Inset* Cleavage furrow). Mitochondria in daughter two-cell blastomeres remained in a large aggregate and occupied the central location of the blastomere with the newly formed nuclei adopting an eccentric position (*Inset* 2 cell).

We extended these observations by labeling MT and DNA to examine the process of mitotic spindle formation and cell division more closely. In controls, NEBD leads to the formation of two closely opposed minispindles harboring maternal and paternal chromosomes as shown previously (47). These rapidly merged into a single spindle before proceeding to anaphase (Fig. 5*F*, *Top*, Movie S3). In

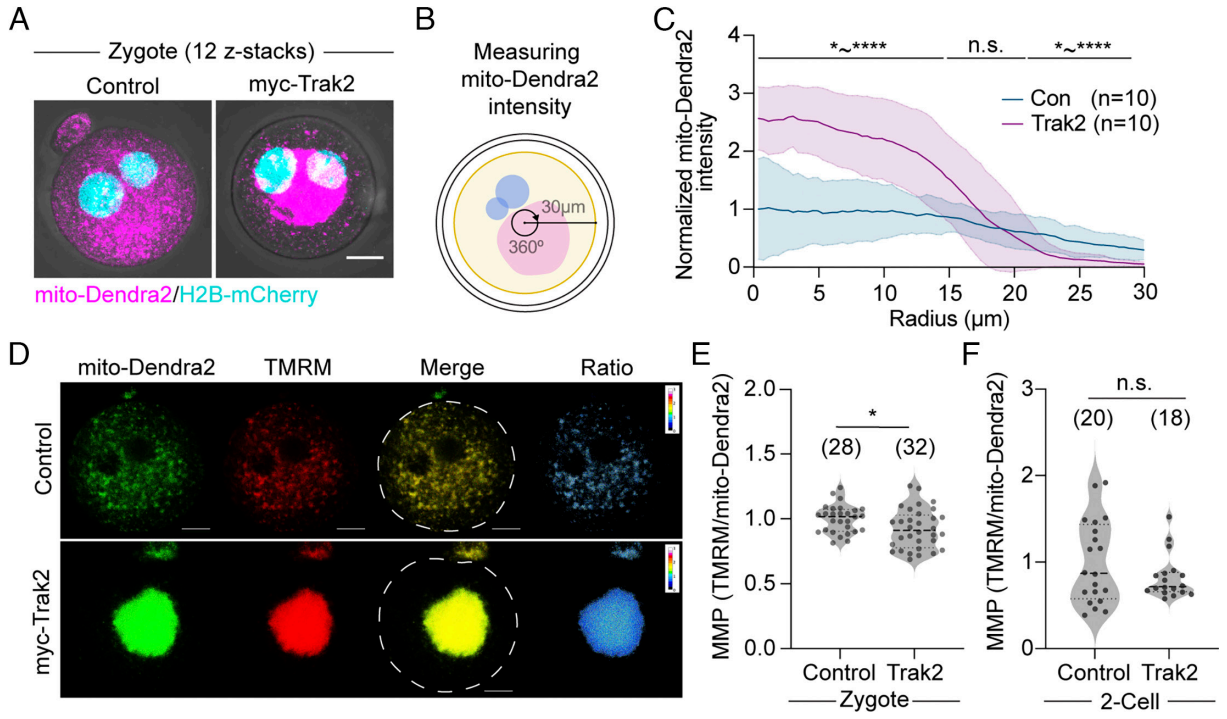

Fig. 4. In zygotes *Trak2* induces a ball-like mitochondrial aggregate that self-centers in the cytoplasm. (*A*) Representative images (12 stacks of z-projection) of mitochondria in control and *Trak2*-expressing zygotes. (*B*) Schematic illustrating the method for measuring cytoplasmic mitochondrial distribution. Magenta: Mitochondria, Blue: PN, Yellow: ROI indicating where mito-Dendra2 were measured. (*C*) Measurement of normalized mito-Dendra2 intensity. Multiple unpaired *t* test. (*D*) Representative images of control and *Trak2*-injected zygotes showing TMRM and mito-Dendra2. The *Right* hand panel shows a pseudocolored ratiometric image obtained from TMRM and mito-Dendra2. (*E* and *F*) Quantification of the TMRM to mito-Dendra2 ratio at zygotes and two-cell embryos. The data were normalized by dividing the values of each group by the mean of the control. Unpaired *t* test. Zygotes were collected from 3-wk-old mice. The scale bar is 15 µm (*A* and *D*). n.s. not significant. *$P < 0.05$ ~ ****$P < 0.0001$.

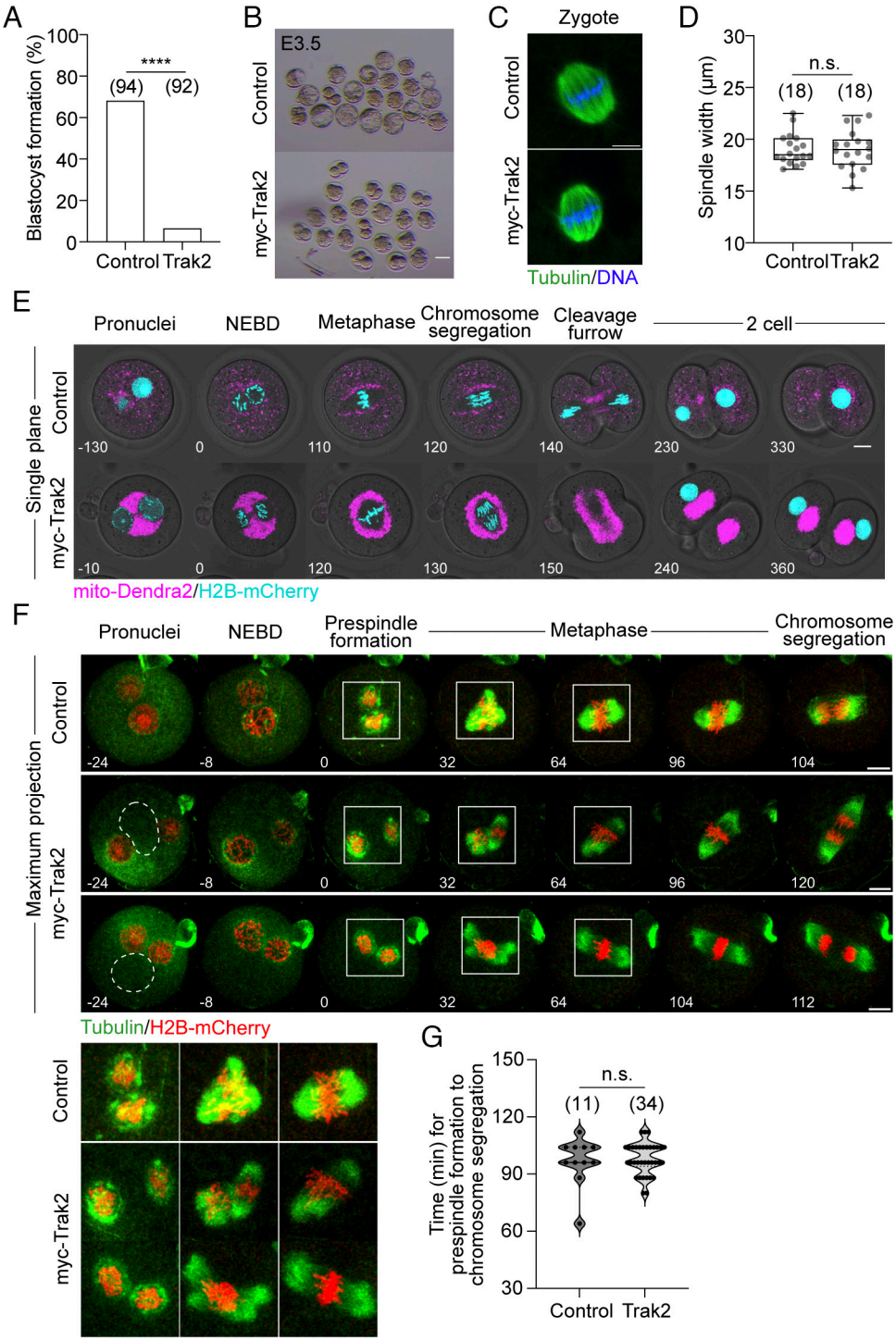

Fig. 5. *Trak2*-induced mitochondrial aggregation inhibits preimplantation development. (*A*) *Trak2*-injected zygotes were cultured to the two-cell stage, and the percentage of two-cells forming blastocysts is shown. Chi-square test. (*B*) Differential interference contrast images of embryos at 3.5 dpc. (*C*) Representative images of the first mitotic spindles in control and *Trak2*-expressing zygotes. (*D*) Measurement of the width of the spindle in the zygote after *Trak2* expression. Unpaired *t* test. (*E*) Time-lapse images of chromosomes (H2B-mCherry) and mitochondrial (mito-Dendra2) distribution during the first mitotic division on the single plane. Note the chromosomes center within the mitochondrial mass during metaphase. Time is presented in minutes relative to chromosome condensation. (*F*) The first mitotic spindle formation in control or *Trak2*-injected zygotes. Dashed line; position of the mitochondrial aggregate. *Top* panel: a control zygote. *Middle* panel: a zygote in which two PN are separated by the mitochondrial aggregate. *Bottom* panel: a zygote in which two PN are located close to each other at the edge of the mitochondrial aggregate. *Bottom Left* panel: higher magnification of regions in white squares to better illustrate the merging of prespindles to form a single metaphase spindle. Time: minutes relative to the first image after NEBD. Maximum projection is shown of 18 z-scans at 2.5-um intervals. (*G*) Quantification of time from prespindle formation to chromosome aggregation. Unpaired *t* test. Zygotes were collected from 3-wk-old mice. The scale bar is 15 µm (*D* and *F*). n.s. not significant. ****$P < 0.0001$.

Trak2-injected zygotes, if the PN are separated by the mitochondrial aggregate (Fig. 5*F*, *Middle*, Movie S4), they form two distinct minispindles at the site of NEBD, that then migrate to the zygote center where they merge into a single spindle. In the second example, PN are proximal to each other at the edge of the mitochondrial ball (Fig. 5*F*, *Bottom*, Movie S5). At NEBD, similar to controls, two minispindles begin forming and combine within the 8 min between images. The spindle then migrates to occupy the oocyte center, presumably within the mitochondrial mass as shown above in Fig. 5*E*. Despite these different approaches to spindle formation there was no detectable difference in the timing of progression from the first sign of prometaphase MT polymerization at the chromosomes to anaphase onset (Fig. 5*G*).

Mitochondrial Aggregation Disrupts Central Nuclear Positioning in Two-Cell Embryos. Given cell division of the zygote was not impeded by the mitochondrial mass, we investigated why *Trak2*-injected embryos may fail to develop. We undertook a detailed analysis of the features of the blastomeres and nuclei in two-cell embryos derived from control and *Trak2*-expressing zygotes (Fig. 6*A*). First, we measured the size of the daughter blastomeres and found that the symmetry of cell division was compromised in *Trak2*-expressing zygotes, as indicated by a greater variance in the size of daughter blastomeres compared to controls (Fig. 6 *B* and *C*).

Similar to zygotes, the mitochondrial mass in two-cell blastomeres remained aggregated into a single structure and showed self-centering properties, leading to the displacement of the nucleus

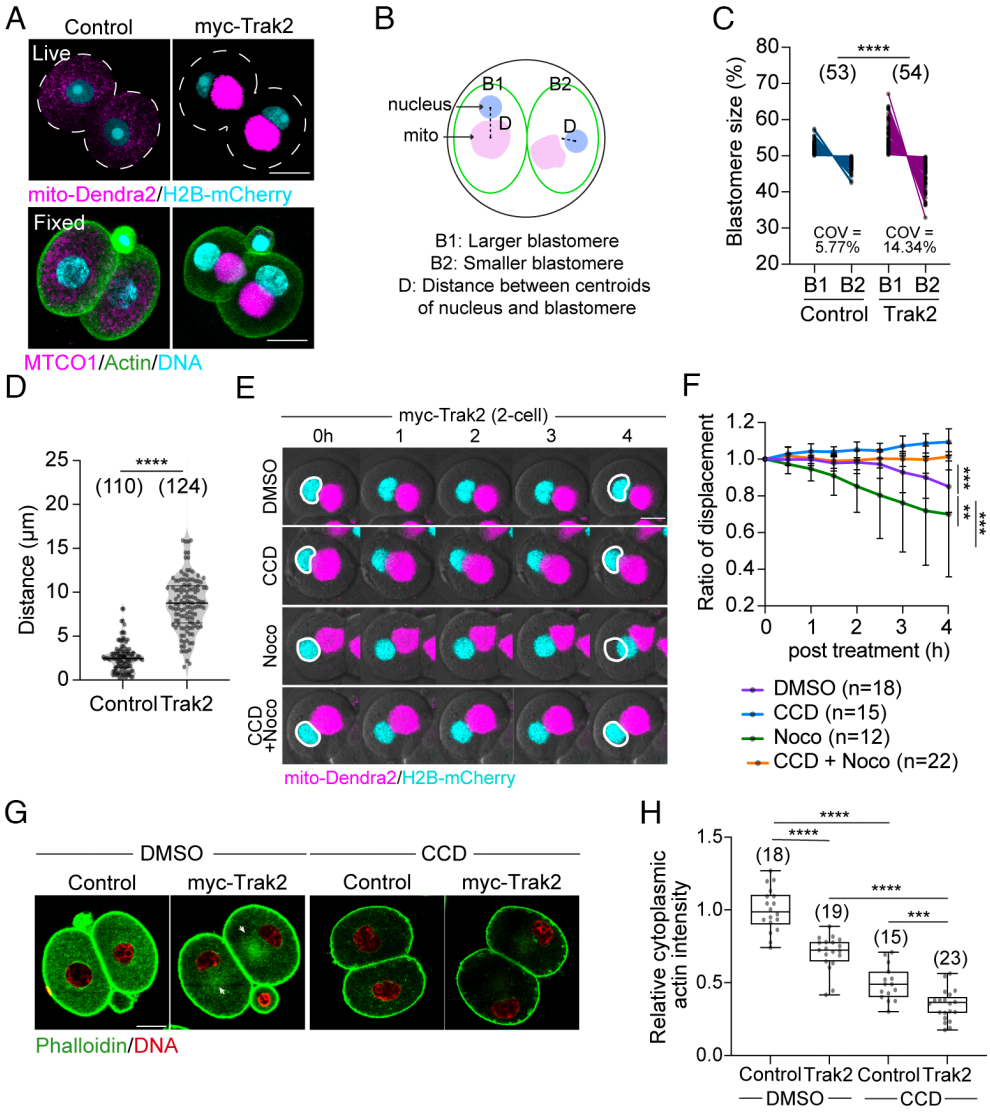

Fig. 6. The nucleus and the mitochondrial aggregate induced by *Trak2* compete for the central position in two-cell embryos. (*A*) Representative images of mitochondrial and nuclear localization in live (*Top*) and fixed (*Bottom*) two-cell embryos. (*B*) A schematic diagram illustrating the analysis performed to measure blastomere size in (*C*) and nuclear displacement in (*D*). (*C*) Measurement of blastomere size in control and *Trak2*-expressing two-cell embryos. Coefficient of variation, F-test to compare variances. (*D*) Measurement of the distance between the centroids of the nucleus and the blastomere. Unpaired *t* test. (*E*) Time-series images of nuclear positioning in *Trak2* expressing two-cell embryos after treatment with Cytochalasin D (CCD) or/and Nocodazole (Noco). The nuclear position at the start of the 4 h imaging period is shown in the first and last images of each time series. (*F*) Measurement of normalized displacement of the nucleus from the initial localization (0 h). Simple linear regression. Data are represented as mean ± SD. Slope value in DMSO −0.025, CCD 0.029, Noco −0.07, and CCD+Noco 0.003. (*G*) Representative images of actin filaments in control and *Trak2*-expressing two-cell embryos after treatment with or without CCD. (*H*) Measurement of the cytoplasmic actin intensity. Unpaired *t* test. Zygotes were collected from 3-wk-old mice. The scale bar is 20 µm (*A* and *G*). ***$P < 0.001$ and ****$P < 0.0001$.

toward the periphery of the blastomere (Fig. 6*A*). To quantify the extent of nuclear displacement, we measured the distance between the centroids of the blastomere and the nucleus. This analysis revealed a threefold to fourfold increase in nuclear displacement in blastomeres of *Trak2*-injected zygotes compared to controls (Fig. 6 *B* and *D*).

We next examined the relative contributions of the actin and MT cytoskeleton to nuclear displacement in two-cell blastomeres (Fig. 6 *E* and *F*). In *Trak2*-expressing controls, there was a gradual nuclear migration toward the center that accelerated just prior to mitosis, similar to the late chromosome centration seen in zygotes just prior to the onset of anaphase. On depolymerization of actin filaments, nuclear centration did not progress, and displacement toward the periphery increased, suggesting that nuclear centering is driven by an actin force (48). Conversely, inhibition of MT polymerization enhanced nuclear centering. We interpret this as nocodazole inhibiting MT-mediated centering of the mitochondrial mass, thereby enabling actin-mediating nuclear centering.

To further examine the relationship between actin, mitochondria, and nuclear centration, zygotes were injected with *Trak2* mRNA and stained with phalloidin after cleavage to the two-cell stage. Consistent with data shown above (Fig. 6 *E* and *F*), nuclei in *Trak2*-injected embryos were oriented toward the cortex, and inhibition of actin led to further displacement (Fig. 6*G*). Interestingly, mitochondrial aggregation significantly reduced the amount of cytoplasmic actin in both untreated and CCD-treated embryos (Fig. 6*H*). This may in part be caused by an accumulation of actin in the mitochondrial aggregate (white arrows in Fig. 6 *G* and *H*). These findings indicate that the spatial organization of mitochondria influences the extent of cytoplasmic actin polymerization, which in turn may contribute to the reduced centering force acting on nuclei, thereby further permitting dominance of the mitochondrial aggregate in the bid for centration.

Mitochondrial Aggregation Distorts Nuclear Shape in Two-Cell Embryos. We also observed that the structure of nuclei in two-cell embryos appeared disrupted in the presence of the mitochondrial mass (Fig. 7*A*). Assessment of nuclear shape (Fig. 7*B*) revealed that the presence of aggregated mitochondria caused increased distortion to nuclear morphology (Fig. 7*C*), resulting in an increased elliptical shape (Fig. 7 *D* and *E*). Moreover, close analysis of nuclei revealed the presence of nuclear "buds," defined here as micronuclei (MN), which were increased by over threefold in the presence of aggregated mitochondria (Fig. 7*F*). Overall, these findings demonstrate that mitochondrial aggregation leads to defects in nuclear integrity by physically disrupting the nuclear structure.

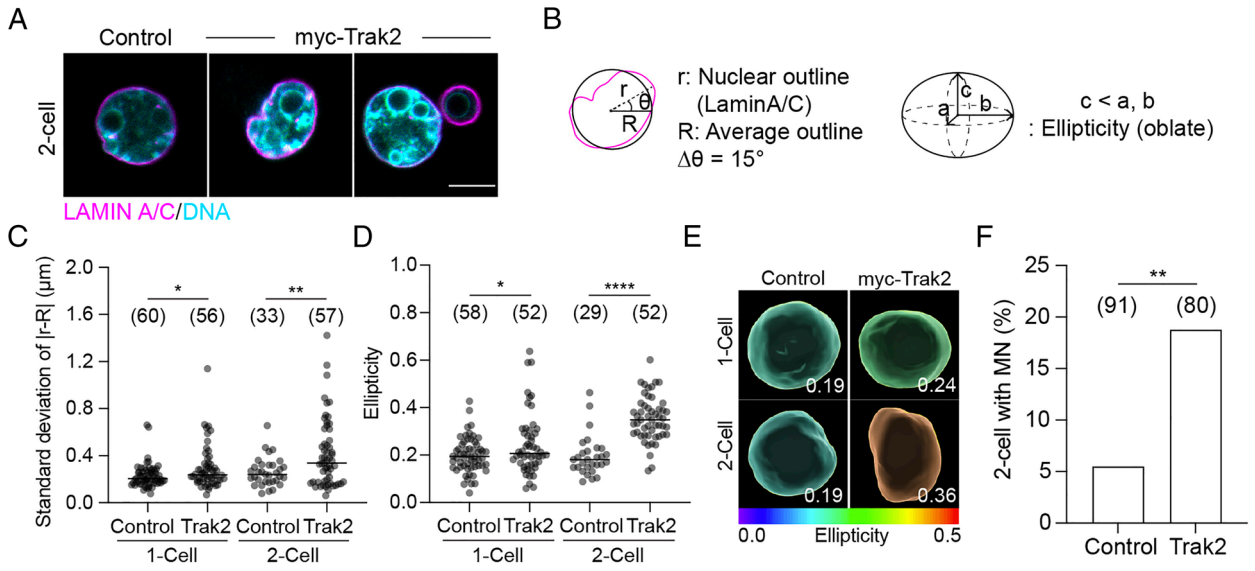

Fig. 7. *Trak2*-induced mitochondrial mass distorts nuclear morphology. (*A*) Representative images of nuclear structure in two-cell stage embryos. Note the presence of MN in the *Bottom* panel. (*B*) Schematic diagrams illustrating the measurement of the distance between the nuclear centroid and nuclear outline (r) and the perfect circle based on the average outline (R) of control one- and two-cell stage embryos and illustrating the measurement of ellipticity. (*C*) The displaced distance of the nuclear outline from the perfect circle was measured and shown as the SD. Unpaired *t* test. (*D* and *E*) Measurement of nuclear ellipticity in one- and two-cell stage embryos. Unpaired *t* test. (*F*) The percentage of two-cell stage embryos containing MN. Chi-square test. Zygotes were collected from 3-wk-old mice. The scale bar is 10 μm (*A*). **P* < 0.05, ***P* < 0.01, and *****P* < 0.0001.

DNA Synthesis and Global RNA Transcription Are Compromised in Two-Cell Blastomeres with Aggregated Mitochondria. Given the impact of aggregated mitochondria on nuclear position and shape in two-cell embryos, we decided to investigate aspects of nuclear function, including DNA synthesis, DNA damage, transcription, and epigenetic modifications. DNA replication as measured by EdU (5-ethynyl-2′-deoxyuridine) incorporation was significantly reduced (Fig. 8 *A* and *B*), while DNA damage, as indicated by γH2AX labeling, was significantly increased in the presence of aggregated mitochondria (Fig. 8 *C* and *D*). Global transcription at the two-cell stage provides a measure of the initiation of embryonic genome activation (EGA), which is essential for embryonic development (49). Embryos with aggregated mitochondria had significantly reduced incorporation of h 5-EU (5′-ethynyluridine), indicating decreased transcription and a faulty EGA (Fig. 8 *E* and *F*). Furthermore, DNA methylation in the form of 5-methylcytosine (5mC) and 5-hydroxymethylcytosine (5hmC) was significantly increased in the nuclei of blastomeres

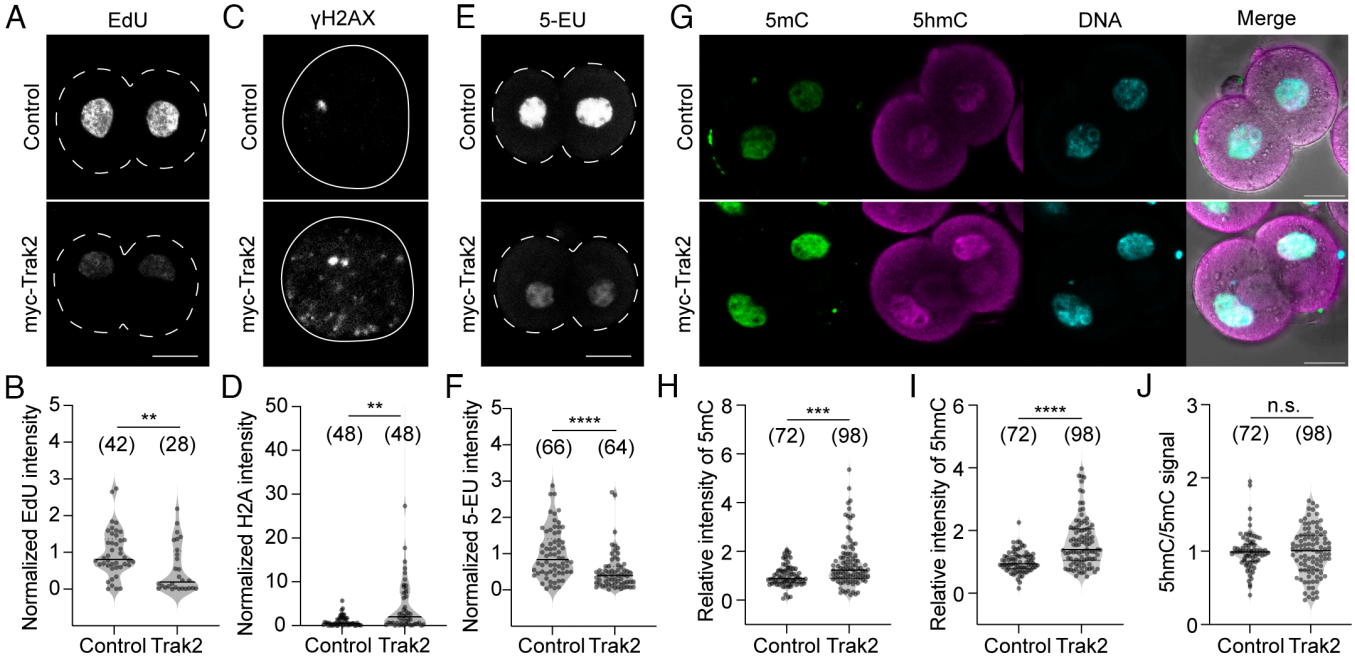

Fig. 8. Mitochondrial aggregation suppresses DNA synthesis and global RNA transcription in two-cell embryos. (*A*) Representative images of EdU signals in two-cell embryos. Dashed line: Cell membrane. (*B*) Normalized intensity of EdU signals. Unpaired *t* test. (*C*) Representative image of γH2AX signals in two-cell embryos. White line: Nuclear outline. (*D*) Normalized intensity of γH2AX signals. Unpaired *t* test. (*E*) Representative images of 5-EU signals in control and *Trak2*-expressing two-cell embryos. Dashed line: Cell membrane. (*F*) Normalized intensity of 5-EU signals. Unpaired *t* test. (*G*) Representative images of 5mC and 5hmC in control and *Trak2*-expressing two-cell embryos. (*H* and *I*) Normalized intensity measurements of 5mC and 5hmC, respectively. Unpaired *t* test. (*J*) Comparison of 5hmC/5mC ratio in two-cell stage embryo control and *Trak2*-injected embryos. Unpaired *t* test. Zygotes were collected from 3-wk-old mice. The scale bar is 20 μm (*A* and *E*) or 15 μm (*G*). n.s.; not significant. ***P*< 0.01, ****P* < 0.001, and *****P* < 0.0001.

with aggregated mitochondria, which may contribute to the overall decrease in global transcription (Fig. 8 *G–J*). Together, these findings demonstrate that an aggregated mitochondrial distribution leads to a myriad of defects in nuclear function that likely underlie the failure of preimplantation development.

Discussion

Here, we show that preventing the normal diffuse distribution of mitochondria has dramatic effects on the organization of mitotic cell divisions of the early embryo, ultimately leading to failure of preimplantation development. In contrast, the asymmetric meiotic cell divisions of the oocyte were relatively untouched by mitochondrial aggregation.

A delay in GVBD was the one significant impact on meiotic progression. The mechanism is unclear, but GVBD is driven by nuclear import of Cyclin B (50, 51), a process that may be impeded by aggregation of mitochondria around the GV. Subsequent meiotic events of spindle formation and polar body extrusion appeared unimpeded. This is consistent with the asymmetric architecture of the meiotic cell divisions where clearance of mitochondria from the cortical end of the spindle just prior to anaphase (14) leads to an effective separation of the mitochondrial mass from the events of polar body extrusion. These findings also suggest *Trak2* expression specifically targets mitochondrial distribution, with little to no effect on MMP, or other cellular events sensitive to motor protein activity, such as spindle formation, even when extending the *Trak2* expression time out to 24 h. Unlike TRAK2, other proteins known to disrupt mitochondrial disruption such as MFN2 (mitofusin2), cause spindle disruption and abnormal chromosome segregation (41), likely as a result of diverse effects on mitochondrial dynamics and mitochondrial function (52, 53). Thus, *Trak2* expression appears to be an excellent tool to specifically examine the effects of mitochondrial distribution in cells with minimal impact on other cellular events.

The lack of impact of disrupted mitochondrial distribution on meiosis contrasts with its effects on mitotic events postfertilization. *Trak2*-mediated mitochondrial aggregation in zygotes was permissive of cell division to the two-cell stage, albeit with an increase in asymmetry in blastomere size and increased presence of MN in two-cell embryos. The basis of these effects likely arises from the mitochondrial mass occupying the zygote center, displacing the PN prior to cell division and thereby compromising the fidelity of the symmetry of cell division.

Despite this disrupted architecture, a relatively normal mitotic progression is enabled by a powerful spindle-centering mechanism revealed in our experiments. Normally, NEBD takes place after PN are apposed at the center of the zygote leading to a centrally placed mitotic spindle. However, in the presence of aggregated mitochondria, the displaced and often separated PN led to the formation of distinct minispindles of paternal and maternal chromosomes (47). These spindles rapidly fused as they became centered in the zygote, and in the process became embedded within the mitochondrial mass. The finding that the mitochondrial mass is no barrier to centration of the mitotic apparatus, indicates that there are mechanisms active in metaphase that ensure that the spindle is centered in the zygote cytoplasm.

The failure of nuclear positioning provides insights into why it is important for cells to maintain a diffuse mitochondrial distribution. The presence of aggregated mitochondria results in MT-mediated competition for the cell center such that in the face of motor protein-mediated forces on mitochondria, actin-mediated positioning of the nucleus is unable to compete. Our data on manipulating the cytoskeleton in *Trak2* expressing embryos support this model of nuclear centration in that MT depolymerization promotes nuclear centering, while inhibition of actin exacerbates nuclear displacement toward the cell periphery. These findings are consistent with MTs being the predominant mode of mitochondrial trafficking (3), while actin is known to be responsible for nuclear centering in one- and two-cell embryos (48, 54–57).

Our findings also revealed that actin accumulates in the mitochondrial aggregate and there is a concomitant reduction in cytoplasmic actin, an effect that likely exacerbates mitochondrial centration and nuclear displacement discussed above. The mechanism of this change in cytoplasmic actin distribution may be a result of mitochondria harboring actin nucleators such as Spire (58). Actin polymerization at mitochondria is known to be important for promoting mitochondrial fission (2), but our findings suggest the dispersed distribution of mitochondria also contributes to the normal coordination of cytoplasmic actin polymerization.

In addition to disrupting nuclear position, the cytoskeletal forces acting on aggregated mitochondria also led to significant disruption of nuclear morphology and function. This disruption was evident in alterations in DNA synthesis, our data do not distinguish between delayed or inhibited DNA replication, increased DNA damage, and the failure to ramp up transcription as required for EGA. Interestingly, we also found that 5mC and 5hmC levels were increased, pointing to an overall higher methylation level that is consistent with the suppression of transcription (59, 60). The fact that the first, but not the second, mitotic division occurs independently of transcription (61) may also explain their different sensitivities to mitochondrial aggregation. Our findings align with recent studies showing that mechanical disruption of nuclear shape and/or localization causes alterations in chromatin structure, changes in gene expression, and compromised genome stability (62–66). Taken together, a major conclusion from the present study is that maintaining a dispersed mitochondrial distribution is needed to enable optimal nuclear position and function, thereby ensuring optimal developmental potential.

Our findings also suggest developmental changes in the activity of motor proteins in oocytes and early embryos. Previously, we have demonstrated active +end kinesin- and dynein-mediated trafficking of mitochondria in oocytes (14). Here, we have identified a size-dependent transition from primarily dynein-mediated trafficking (perinuclear aggregation) to one that utilizes both dynein and kinesin (cortical and perinuclear aggregation). This initial dynein-dominated trafficking in small oocytes may be a reflection of Balbiani-like structures of aggregated mitochondria in growing oocytes (32, 67–69). Interestingly, TRAK2 (Milton) is essential for Balbiani body in Drosophila oocytes (32) and the formation of "mitoballs" in primary Drosophila spermatocytes (70).

Furthermore, after fertilization, mitochondria exclusively aggregate in the center of the zygote and two-cell blastomeres, with no evidence of cortical accumulation. One possible explanation for the dominance of dynein-mediated trafficking may be the postfertilization upregulation of dynein-binding protein Lissencephaly-1 (LIS1). LIS1 expression has been suggested to promote pronuclear motility and genomic union in mammalian zygotes (71) and has recently been shown to switch TRAK2-mediated trafficking kinesin to dynein (29). The upregulation of LIS1 after fertilization may explain the transition from bidirectional mitochondrial trafficking in oocytes to unidirectional trafficking in embryos.

In summary, we show that disrupting mitochondrial distribution has dramatic effects on nuclear position, shape, and function that ultimately lead to the failure of preimplantation development.

Our findings have implications for understanding infertility resulting from poor embryo development. Successful preimplantation embryo development is reliant on the fidelity of the first cleavage divisions and IVF pregnancy rates are dramatically reduced if embryos have varying blastomere sizes (72–74). Thus, mechanisms to ensure appropriate organelle distribution and cytoplasmic architecture that enable normal nuclear centering and nuclear function are critical for successful development.

Materials and Methods

Mice. C57B6/J or PhAM female mice (75) were used in this study. *PhAM^{floxed}* mice were crossed with transgenic male mice carrying *Gdf-9* promoter-mediated Cre recombinase (76). Homozygous PhAM female mice contain a mitochondrially localized photoconvertible fluorescent protein Dendra2 (mito-Dendra2) specifically in oocytes. Mice were housed under controlled environmental conditions where water and food were provided ad libitum. All animal experiments were approved by Monash University Animal Ethics Committee and were performed in accordance with Australian National Health and Medical Research Council Guidelines on Ethics in Animal Experimentation.

Oocytes and Fertilized Zygote Collection and Culture. GV oocytes were collected from ovaries of 3 or 6 wk-old female mice previously primed (44 to 48 h) with an intraperitoneal injection of pregnant mare's serum gonadotropin (10 IU PMSG, Intervet). M2 medium contained 200 μm of 3-isobutyl-1-methylxanthine (M2+IBMX; Sigma-Aldrich) used for oocyte collection to inhibit spontaneous cell cycle resumption. Cumulus–oocyte complexes were repeatedly pipetted using a narrow-bore glass pipette to remove cumulus cells surrounding fully grown GV oocytes. For in vitro maturation, GV oocytes were washed in fresh M16 medium (Sigma-Aldrich) before being transferred to drops of the same medium covered with mineral oil (Sigma-Aldrich) in an incubator at 37 °C (5% CO_2 in air). MI oocytes were collected about 6 to 7 h after the resumption of meiosis, and metaphase II oocytes with the first polar bodies were collected about 12 h after GVBD.

Fertilized zygotes were collected from the oviducts after human chorionic gonadotropin (hCG, 10 IU; Sigma-Aldrich) injection at 44 to 48 h post PMSG stimulation and mated with stud F1 male mice. The mice were culled 20 to 22 h after hCG injection to harvest zygotes from oviducts. Zygote were in vitro cultured in SAGE-1 Step medium (CooperSurgical) covered with mineral oil in the incubator at 37 °C (5% CO_2 in air).

In Vitro Transcription and Microinjection. To generate the capped mRNAs, the linearized plasmid templates were transcribed in vitro using a mMessage mMachine SP6, or T7 kit (Invitrogen) according to the manufacturer's instructions. Poly-A tails were added using a poly-A Tailing kit (Invitrogen). In vitro transcripts were purified using an RNeasy® Mini kit (Qiagen) and stored at −80 °C until use: *myc-Trak2* (300 ng/μL), *Trak2-EGFP* (300 ng/μL), *myc-Trak2-KDM* (600 ng/μL), *mtPA-GFP* (1,000 ng/μL), *H2B-mCherry* (300 ng/μL), or *EGFP* (500 ng/μL).

GV oocytes or zygotes were microinjected with mRNAs using an MMN-1 coarse micromanipulator (Narishige). A holding pipette (Gytech) was used to position oocytes/zygotes for microinjection, and a micropipette (Harvard Apparatus) pulled by a vertical pipette puller (Sutter Instruments) was inserted into the cytoplasm. An intracellular electrometer allowed a brief pulse of negative capacitance to assist the pipette tip to breach the membrane. mRNAs were delivered to the cytoplasm using a fixed-pressure pulse through a PV820 pneumatic picopump (World precision instruments). Microinjection volume was estimated at 5% by cytoplasmic displacement. Following microinjection, oocytes/zygotes were allowed to recover in fresh drops of M2 medium covered by mineral oil at room temperature for 10 min.

Mitochondrial Staining for Live Cell Imaging. Oocytes/zygotes were cultured in M2 medium supplemented with 25 nM Tetramethylrhodamine, Methyl Ester, Perchlorate (TMRM, Sigma-Aldrich) at 37 °C for 30 min or 100 nM Mitotracker Red FM (Invitrogen) at 37 °C for 30 min. Eggs were transferred to drops of M2 medium on a round coverslip inserted into a 35 mm metal chamber. TMRM, Mitotracker, or mito-Dendra2 signal was captured using an inverted Leica SP8 confocal microscope equipped with a temperature-controlled incubation box. Single plane snaps or full z-stacks of whole oocytes at 1 to 2 μm intervals were imaged. Images were processed for the frame alignment using an "Image Stabilizer" plugin (77) written in FIJI before analysis.

Tubulin Staining for Live Cell Imaging. Zygotes were cultured in M2 medium supplemented with 200 nM abberior Tubulin-LIVE 610 dye (Abberior) at 37 °C for 30 min and were transferred to drops of M2 medium containing with 100 nM Tubulin-LIVE 610 dye on a round coverslip inserted into a 35 mm metal chamber. The signal was captured using a Zeiss LSM 980 confocal microscope equipped with a temperature-controlled incubation box. Z-stacks at 2.5-μm intervals were imaged.

Immunofluorescence. Oocytes/fertilized embryos were fixed in 4% paraformaldehyde (PFA; Sigma-Aldrich) containing 0.5% Triton X-100 (Sigma-Aldrich) for 30 min at room temperature. For 5mC and 5hmC labeling in two-cell embryos, zona pellucida was removed by Tyrode's solution acidic (Sigma-Aldrich). Eggs were fixed in 4% PFA for 20 min and then denatured with 4 N hydrochloric acid (HCl) for 10 min, neutralized with 100 mM Tris-HCl (pH 8.5) for 10 min. After 1 h of blocking in 3% bovine serum albumin (Sigma-Aldrich) in phosphate-buffered saline (PBS), oocytes/embryos were stained with the primary antibodies overnight at 4 °C; MTCO1 (ab14705, Abcam), CREST (90C-CS1058, Fitzgerald), LAMIN A/C (#4777, Cell signaling), 5mC (MCA2201, Bio-Rad), and 5hmC (#39069, Active motif). This was followed by incubation with specific Alexa Fluor secondary antibodies (Invitrogen). Tubulin was stained with Alexa-Fluor-488-alpha tubulin (#322588, Invitrogen). F-actin was stained with Alexa Fluor Plus 555 Phalloidin (A30106, Invitrogen). DNA was labeled by Hoechst 33342 (10 μg/mL; Sigma-Aldrich) for 10 min at room temperature. Images were acquired using an inverted Leica SP8 confocal microscope or a Zeiss LSM 980 confocal microscope with a 40× water or 63× water immersion objective and analyzed using FIJI.

EdU and 5-EU Incorporation. Two-cell embryos were incubated with 2 mM EU (5-Ethynyl Uridine, Invitrogen) to detect global RNA transcription for 2 h or 50 μm Edu (Invitrogen) to measure active DNA synthesis for 12 h in SAGE-1 step medium. Two-cell embryos were fixed in 4% PFA and permeabilized with 0.5% Triton X-100 for 30 min then stained using the Click-iT assay kit (Thermo Fisher Scientific) according to the manufacturer's instructions.

Statistical Analysis. Statistical analysis of experiments with two groups was carried out using an unpaired *t* test. The Chi-square (and Fisher's exact) test was used to compare the percentage of meiotic resumption, first polar body extrusion, cortical mitochondria, blastocyst formation, and MN formation. Multi unpaired *t* test was used for mitochondrial intensity analysis in zygotes. F-test was used to compare variances in the blastomere size. * denotes a *P*-value of <0.05, ** denotes a *P*-value of <0.01, *** denotes a *P*-value of <0.001, and **** denotes a *P*-value of <0.0001. On the violin and whisker plots, the central line indicates the median, and the top and bottom of the line indicate 25% and 75%. Data were collated from three independent experimental replicates.

Data, Materials, and Software Availability. All study data are included in the article and/or supporting information.

ACKNOWLEDGMENTS. We thank Prof. Josef Kittler (University College London) for providing the plasmids used in this study. We also thank Monash Animal Research Platform and Monash Micro Imaging platform for their support in enabling the experiments performed herein. This study was funded by National Health and Medical Research Council (NHMRC) Australia (grant number 1165627) and NHMRC (grant number 200112).

Author affiliations: [a]Department of Anatomy and Developmental Biology, Monash Biomedicine Discovery Institute, Monash University, Clayton, VIC 3800, Australia

1. P. Mishra, D. C. Chan, Mitochondrial dynamics and inheritance during cell division, development and disease. *Nat. Rev. Mol. Cell Biol.* **15**, 634–646 (2014).
2. F. Kraus, K. Roy, T. J. Pucadyil, M. T. Ryan, Function and regulation of the divisome for mitochondrial fission. *Nature* **590**, 57–66 (2021).
3. T. L. Schwarz, Mitochondrial trafficking in neurons. *Cold Spring Harb. Perspect. Biol.* **5**, a011304 (2013).
4. O. A. Quintero *et al.*, Human Myo19 is a novel myosin that associates with mitochondria. *Curr. Biol.* **19**, 2008–2013 (2009).
5. J. Y. Chung, J. A. Steen, T. L. Schwarz, Phosphorylation-induced motor shedding is required at mitosis for proper distribution and passive inheritance of mitochondria. *Cell Rep.* **16**, 2142–2155 (2016).
6. G. Kanfer *et al.*, Mitotic redistribution of the mitochondrial network by Miro and Cenp-F. *Nat. Commun.* **6**, 8015 (2015).
7. Z. H. Sheng, Mitochondrial trafficking and anchoring in neurons: New insight and implications. *J. Cell Biol.* **204**, 1087–1098 (2014).
8. M. H. Schuler *et al.*, Miro1-mediated mitochondrial positioning shapes intracellular energy gradients required for cell migration. *Mol. Biol. Cell* **28**, 2159–2169 (2017).
9. S. Madan, B. Uttekar, S. Chowdhary, R. Rikhy, Mitochondria lead the way: Mitochondrial dynamics and function in cellular movements in development and disease. *Front. Cell Dev. Biol.* **9**, 781933 (2021).
10. Z. H. Sheng, Q. Cai, Mitochondrial transport in neurons: Impact on synaptic homeostasis and neurodegeneration. *Nat. Rev. Neurosci.* **13**, 77–93 (2012).
11. X. Zhang, X. Q. Wu, S. Lu, Y. L. Guo, X. Ma, Deficit of mitochondria-derived ATP during oxidative stress impairs mouse MII oocyte spindles. *Cell Res.* **16**, 841–850 (2006).
12. M. T. Johnson, E. A. Freeman, D. K. Gardner, P. A. Hunt, Oxidative metabolism of pyruvate is required for meiotic maturation of murine oocytes in vivo. *Biol. Reprod.* **77**, 2–8 (2007).
13. X. Wang, T. L. Schwarz, The mechanism of Ca2+ -dependent regulation of kinesin-mediated mitochondrial motility. *Cell* **136**, 163–174 (2009).
14. C. M. Dalton, J. Carroll, Biased inheritance of mitochondria during asymmetric cell division in the mouse oocyte. *J. Cell Sci.* **126**, 2955–2964 (2013).
15. U. Al-Zubaidi *et al.*, Mitochondria-targeted therapeutics, MitoQ and BGP-15, reverse aging-associated meiotic spindle defects in mouse and human oocytes. *Hum. Reprod.* **36**, 771–784 (2021).
16. U. Al-Zubaidi *et al.*, The spatio-temporal dynamics of mitochondrial membrane potential during oocyte maturation. *Mol. Hum. Reprod.* **25**, 695–705 (2019).
17. A. S. Moore *et al.*, Actin cables and comet tails organize mitochondrial networks in mitosis. *Nature* **591**, 659–664 (2021).
18. G. Lopez-Domenech *et al.*, Miro proteins coordinate microtubule- and actin-dependent mitochondrial transport and distribution. *EMBO J.* **37**, 321–336 (2018).
19. A. D. Pilling, D. Horiuchi, C. M. Lively, W. M. Saxton, Kinesin-1 and Dynein are the primary motors for fast transport of mitochondria in Drosophila motor axons. *Mol. Biol. Cell* **17**, 2057–2068 (2006).
20. R. L. Morris, P. J. Hollenbeck, Axonal transport of mitochondria along microtubules and F-actin in living vertebrate neurons. *J. Cell Biol.* **131**, 1315–1326 (1995).
21. A. F. MacAskill, J. T. Kittler, Control of mitochondrial transport and localization in neurons. *Trends Cell Biol.* **20**, 102–112 (2010).
22. S. Fransson, A. Ruusala, P. Aspenstrom, The atypical Rho GTPases Miro-1 and Miro-2 have essential roles in mitochondrial trafficking. *Biochem. Biophys. Res. Commun.* **344**, 500–510 (2006).
23. E. E. Glater, L. J. Megeath, R. S. Stowers, T. L. Schwarz, Axonal transport of mitochondria requires milton to recruit kinesin heavy chain and is light chain independent. *J. Cell Biol.* **173**, 545–557 (2006).
24. A. F. Macaskill *et al.*, Miro1 is a calcium sensor for glutamate receptor-dependent localization of mitochondria at synapses. *Neuron* **61**, 541–555 (2009).
25. R. S. Stowers, L. J. Megeath, J. Gorska-Andrzejak, I. A. Meinertzhagen, T. L. Schwarz, Axonal transport of mitochondria to synapses depends on milton, a novel Drosophila protein. *Neuron* **36**, 1063–1077 (2002).
26. K. Brickley, F. A. Stephenson, Trafficking kinesin protein (TRAK)-mediated transport of mitochondria in axons of hippocampal neurons. *J. Biol. Chem.* **286**, 18079–18092 (2011).
27. M. van Spronsen *et al.*, TRAK/Milton motor-adaptor proteins steer mitochondrial trafficking to axons and dendrites. *Neuron* **77**, 485–502 (2013).
28. V. Henrichs *et al.*, Mitochondria-adaptor TRAK1 promotes kinesin-1 driven transport in crowded environments. *Nat. Commun.* **11**, 3123 (2020).
29. A. R. Fenton, T. A. Jongens, E. L. F. Holzbaur, Mitochondrial adaptor TRAK2 activates and functionally links opposing kinesin and dynein motors. *Nat. Commun.* **12**, 4578 (2021).
30. J. T. Canty, A. Hensley, M. Aslan, A. Jack, A. Yildiz, TRAK adaptors regulate the recruitment and activation of dynein and kinesin in mitochondrial transport. *Nat. Commun.* **14**, 1376 (2023).
31. J. Gorska-Andrzejak *et al.*, Mitochondria are redistributed in Drosophila photoreceptors lacking milton, a kinesin-associated protein. *J. Comp. Neurol.* **463**, 372–388 (2003).
32. R. T. Cox, A. C. Spradling, Milton controls the early acquisition of mitochondria by Drosophila oocytes. *Development* **133**, 3371–3377 (2006).
33. L. Piko, K. D. Taylor, Amounts of mitochondrial DNA and abundance of some mitochondrial gene transcripts in early mouse embryos. *Dev. Biol.* **123**, 364–374 (1987).
34. P. May-Panloup *et al.*, Low oocyte mitochondrial DNA content in ovarian insufficiency. *Hum. Reprod.* **20**, 593–597 (2005).
35. J. H. Santos, J. N. Meyer, B. S. Mandavilli, B. Van Houten, Quantitative PCR-based measurement of nuclear and mitochondrial DNA damage and repair in mammalian cells. *Methods Mol. Biol.* **314**, 183–199 (2006).
36. J. Van Blerkom, M. N. Runner, Mitochondrial reorganization during resumption of arrested meiosis in the mouse oocyte. *Am. J. Anat.* **171**, 335–355 (1984).
37. R. Dumollard, M. Duchen, J. Carroll, The role of mitochondrial function in the oocyte and embryo. *Curr. Top. Dev. Biol.* **77**, 21–49 (2007).
38. D. Adhikari, I. W. Lee, W. S. Yuen, J. Carroll, Oocyte mitochondria-key regulators of oocyte function and potential therapeutic targets for improving fertility. *Biol. Reprod.* **106**, 366–377 (2022).
39. S. Nagai *et al.*, Correlation of abnormal mitochondrial distribution in mouse oocytes with reduced developmental competence. *Tohoku J. Exp. Med.* **210**, 137–144 (2006).
40. K. Selesniemi, H. J. Lee, A. Muhlhauser, J. L. Tilly, Prevention of maternal aging-associated oocyte aneuploidy and meiotic spindle defects in mice by dietary and genetic strategies. *Proc. Natl. Acad. Sci. U.S.A.* **108**, 12319–12324 (2011).
41. X. H. Wang, S. Yin, X. H. Ou, S. M. Luo, Increase of mitochondria surrounding spindle causes mouse oocytes arrested at metaphase I stage. *Biochem. Biophys. Res. Commun.* **527**, 1043–1049 (2020).
42. I. W. Lee, D. Adhikari, J. Carroll, Miro1 depletion disrupts spatial distribution of mitochondria and leads to oocyte maturation defects. *Front. Cell Dev. Biol.* **10**, 986454 (2022).
43. M. Wilding *et al.*, Mitochondrial aggregation patterns and activity in human oocytes and preimplantation embryos. *Hum. Reprod.* **16**, 909–917 (2001).
44. Y. Gao *et al.*, Protein expression landscape of mouse embryos during pre-implantation development. *Cell Rep.* **21**, 3957–3969 (2017).
45. W. Zheng, H. Zhang, K. Liu, The two classes of primordial follicles in the mouse ovary: Their development, physiological functions and implications for future research. *Mol. Hum. Reprod.* **20**, 286–292 (2014).
46. Y. Yu, R. Dumollard, A. Rossbach, F. A. Lai, K. Swann, Redistribution of mitochondria leads to bursts of ATP production during spontaneous mouse oocyte maturation. *J. Cell Physiol.* **224**, 672–680 (2010).
47. J. Reichmann *et al.*, Dual-spindle formation in zygotes keeps parental genomes apart in early mammalian embryos. *Science* **361**, 189–193 (2018).
48. Y. Ye, H. A. Homer, Two-step nuclear centring by competing microtubule- and actin-based mechanisms in 2-cell mouse embryos. *EMBO Rep.* **23**, e55251 (2022).
49. R. M. Schultz, Regulation of zygotic gene activation in the mouse. *Bioessays* **15**, 531–538 (1993).
50. J. Pines, T. Hunter, Human cyclins A and B1 are differentially located in the cell and undergo cell cycle-dependent nuclear transport. *J. Cell Biol.* **115**, 1–17 (1991).
51. P. Marangos, J. Carroll, The dynamics of cyclin B1 distribution during meiosis I in mouse oocytes. *Reproduction* **128**, 153–162 (2004).
52. H. Chen *et al.*, Mitofusins Mfn1 and Mfn2 coordinately regulate mitochondrial fusion and are essential for embryonic development. *J. Cell Biol.* **160**, 189–200 (2003).
53. R. Filadi, D. Pendin, P. Pizzo, Mitofusin 2: From functions to disease. *Cell Death Dis.* **9**, 330 (2018).
54. G. Schatten *et al.*, Latrunculin inhibits the microfilament-mediated processes during fertilization, cleavage and early development in sea urchins and mice. *Exp. Cell Res.* **166**, 191–208 (1986).
55. A. Chaigne *et al.*, F-actin mechanics control spindle centring in the mouse zygote. *Nat. Commun.* **7**, 10253 (2016).
56. P. Chugh *et al.*, Actin cortex architecture regulates cell surface tension. *Nat. Cell Biol.* **19**, 689–697 (2017).
57. K. Scheffler *et al.*, Two mechanisms drive pronuclear migration in mouse zygotes. *Nat. Commun.* **12**, 841 (2021).
58. U. Manor *et al.*, A mitochondria-anchored isoform of the actin-nucleating spire protein regulates mitochondrial division. *Elife* **4**, e08828 (2015).
59. K. D. Robertson, DNA methylation and human disease. *Nat. Rev. Genet.* **6**, 597–610 (2005).
60. Y. Yin *et al.*, Impact of cytosine methylation on DNA binding specificities of human transcription factors. *Science* **356**, eaaj2239 (2017).
61. P. Braude, V. Bolton, S. Moore, Human gene expression first occurs between the four- and eight-cell stages of preimplantation development. *Nature* **332**, 459–461 (1988).
62. C. Uhler, G. V. Shivashankar, Nuclear mechanopathology and cancer diagnosis. *Trends Cancer* **4**, 320–331 (2018).
63. M. Almonacid *et al.*, Active fluctuations of the nuclear envelope shape the transcriptional dynamics in oocytes. *Dev. Cell* **51**, 145–157.e110 (2019).
64. S. Biedzinski *et al.*, Microtubules control nuclear shape and gene expression during early stages of hematopoietic differentiation. *EMBO J.* **39**, e103957 (2020).
65. Y. Kalukula, A. D. Stephens, J. Lammerding, S. Gabriele, Mechanics and functional consequences of nuclear deformations. *Nat. Rev. Mol. Cell Biol.* **23**, 583–602 (2022).
66. A. Al Jord *et al.*, Cytoplasmic forces functionally reorganize nuclear condensates in oocytes. *Nat. Commun.* **13**, 5070 (2022).
67. R. T. Cox, A. C. Spradling, A Balbiani body and the fusome mediate mitochondrial inheritance during Drosophila oogenesis. *Development* **130**, 1579–1590 (2003).
68. M. E. Pepling, J. E. Wilhelm, A. L. O'Hara, G. W. Gephardt, A. C. Spradling, Mouse oocytes within germ cell cysts and primordial follicles contain a Balbiani body. *Proc. Natl. Acad. Sci. U.S.A.* **104**, 187–192 (2007).
69. L. Lei, A. C. Spradling, Mouse oocytes differentiate through organelle enrichment from sister cyst germ cells. *Science* **352**, 95–99 (2016).
70. A. Y. Z. Li *et al.*, Milton assembles large mitochondrial clusters, mitoballs, to sustain spermatogenesis. *Proc. Natl. Acad. Sci. U.S.A.* **120**, e2306073120 (2023).
71. C. Payne, J. C. St John, J. Ramalho-Santos, G. Schatten, LIS1 association with dynactin is required for nuclear motility and genomic union in the fertilized mammalian oocyte. *Cell Motil. Cytoskeleton* **56**, 245–251 (2003).
72. K. Hardy *et al.*, From cell death to embryo arrest: Mathematical models of human preimplantation embryo development. *Proc. Natl. Acad. Sci. U.S.A.* **98**, 1655–1660 (2001).
73. T. Cavazza *et al.*, Parental genome unification is highly error-prone in mammalian embryos. *Cell* **184**, 2860–2877.e2822 (2021).
74. C. E. Currie *et al.*, The first mitotic division of human embryos is highly error prone. *Nat. Commun.* **13**, 6755 (2022).
75. A. H. Pham, J. M. McCaffery, D. C. Chan, Mouse lines with photo-activatable mitochondria to study mitochondrial dynamics. *Genesis* **50**, 833–843 (2012).
76. Z. J. Lan, X. Xu, A. J. Cooney, Differential oocyte-specific expression of Cre recombinase activity in GDF-9-iCre, Zp3cre, and Msx2Cre transgenic mice. *Biol. Reprod.* **71**, 1469–1474 (2004).
77. K. Li, The image stabilizer plugin for ImageJ (2008). https://www.cs.cmu.edu/~kangli/code/Image_Stabilizer.html. Deposited 7 February 2008.